applied sciences

MDPI

Article

Two-Stage Optimization of Mobile Energy Storage Sizing, Pre-Positioning, and Re-Allocation for Resilient Networked Microgrids with Dynamic Boundaries

Hongtao Lei [1,2,3,*], Bo Jiang [1,3,*], Yajie Liu [1,3], Cheng Zhu [1,2] and Tao Zhang [1,3]

[1] College of Systems Engineering, National University of Defense Technology, Changsha 410073, China
[2] National Key Laboratory of Information Systems Engineering, National University of Defense Technology, Changsha 410073, China
[3] Hunan Key Laboratory of Multi-Energy System Intelligent Interconnection Technology, Changsha 410073, China
* Correspondence: leihongtao@nudt.edu.cn (H.L.); jiangbo20@nudt.edu.cn (B.J.)

Abstract: Networked microgrids (NMGs) enhance the resilience of power systems by enabling mutual support among microgrids via dynamic boundaries. While previous research has optimized the locations of mobile energy storage (MES) devices, the critical aspect of MES capacity sizing has been largely neglected, despite its direct impact on costs. This paper introduces a two-stage optimization framework for MES sizing, pre-positioning, and re-allocation within NMGs. In the first stage, the capacity sizing and pre-positioning of MES devices are optimized before a natural disaster. In the second stage, the re-allocation and active power output of MES devices are adjusted post-disaster, with boundary switches operated based on the damage scenarios. The framework restores unserved loads by either forming isolated microgrids using MES or re-establishing connections between microgrids via smart switches. The proposed framework is modeled mathematically and solved using a customized progressive hedging algorithm. Extensive experiments on modified IEEE 33-node and 69-node systems demonstrate the model's effectiveness and applicability in improving system resilience.

Keywords: resilience; networked microgrids; mobile energy storage; sizing; two-stage optimization

check for updates

Citation: Lei, H.; Jiang, B.; Liu, Y.; Zhu, C.; Zhang, T. Two-Stage Optimization of Mobile Energy Storage Sizing, Pre-Positioning, and Re-Allocation for Resilient Networked Microgrids with Dynamic Boundaries. *Appl. Sci.* **2024**, *14*, 10367. https://doi.org/10.3390/app142210367

Academic Editor: Muhammad Aziz

Received: 5 September 2024
Revised: 31 October 2024
Accepted: 6 November 2024
Published: 11 November 2024

Copyright: © 2024 by the authors. Licensee MDPI, Basel, Switzerland. This article is an open access article distributed under the terms and conditions of the Creative Commons Attribution (CC BY) license (https://creativecommons.org/licenses/by/4.0/).

1. Introduction

Today, with the increasing occurrence of natural disasters caused by climate change, the power system, as a vital infrastructure of human society, has faced a growing number of challenges and disruptions from both environmental factors and human activities. This leads huge loss to societal life and work. Between the years 2003 and 2012, the estimated annual cost of power outages caused by severe weather in the United States ranged from USD 18 to 33 billion [1]. In 2021, Texas faced a significant power outage event caused by an unprecedented winter storm, impacting around 4.5 million residential and commercial properties. The resulting financial consequences were estimated to amount to a minimum of USD 195 billion [2]. Therefore, resilient restoration strategies are of great significance for mitigating the adverse effects of natural disasters on the power system.

Due to its ability to autonomously switch between grid-connected and islanded operation modes, microgrids (MGs) offer a promising solution to enhance the resilience of the power system. In recent years, a multitude of research studies have been conducted to enhance the resilience of microgrids, aiming to effectively address the challenges posed by severe weather phenomena. Networked MGs, which encompass the coordination of multiple MG networks within a fixed or dynamic boundary, have been demonstrated to be an optimal approach for enhancing resiliency [3]. NMGs have recently garnered attention in the literature due to their ability to facilitate the exchange and provision of

electricity between MGs, thereby maintaining a balance between the power generation and load [4]. The operational feasibility of NMGs in distribution systems has been demonstrated in [5,6] through the use of a hierarchical control structure. It represents the further development of the application of MGs through the synchronization of multiple MGs, and could be an increasingly crucial way to improve distribution system resilience. Ref. [7] confirms the unique capability of NMGs as distributed systems in enhancing power system resilience during extreme events, particularly in smart cities. Since the centralized energy management system (EMS) of NMGs obtains all the relevant information of the system and determines the optimum operating point for all network-controlled resources to achieve the global objective [8], we assume that the centralized EMS architecture is implemented for NMGs in this paper.

1.1. Literature Review

In the literature, substantial research has focused on the optimization of NMGs, particularly in the context of enhancing resilience. The typical optimization objectives for resilient NMGs include: (1) increasing supply reliability, such as maximizing power restoration [9] and minimizing unserved loads [10]; (2) reducing system costs, including minimizing both economic costs [11] and outage duration [12]; and (3) minimizing power exchange between microgrids [13]. Different approaches have been proposed to address these objectives. To enhance the operational resilience of hybrid NMGs in emergency mode, Ref. [14] employs an incremental cost consensus algorithm to optimize surplus power distribution among microgrids, effectively reducing load shedding. Ref. [15] focuses on restoring more critical loads by optimizing the scheduling of generation and storage resources within NMGs. Additionally, it introduces a measurement-based risk-limiting strategy to manage the intermittency of renewable energy, thereby improving system reliability. To further address challenges in maintaining resilience under extreme conditions, Ref. [16] tackles reactive power management by proposing a two-stage stochastic programming model based on Here-And-Now and Wait-And-See approaches. This model not only considers load shedding costs, but also incorporates the economic operational costs of the NMGs, offering a more comprehensive approach to resilience optimization. However, many of the aforementioned studies focus on optimizing a single or limited set of objectives, often overlooking the role of network reconfiguration in enhancing resilience. This oversight reduces the overall effectiveness of these strategies in fully addressing the complex dynamics of NMGs during extreme events.

Over the past few years, the potential of connecting mobile emergency generators (MEGs) and MESs to crucial network nodes during emergency scenarios has also been unveiled by many studies, showcasing a promising approach to alleviating load shedding within power system. For instance, the hierarchical scheduling framework proposed in Ref. [17] incorporates mobile units, repair crews, and distribution feeder reconfiguration. The results show a significant improvement in load supply after the integration of mobile units with the network. Additionally, Ref. [18] introduces a decentralized framework for coordinating the dispatch of mobile power sources and repair crews to restore loads. This framework is formulated as a decentralized partially observable Markov decision process and employs a novel hierarchical and hybrid multi-agent reinforcement learning method to demonstrate its effectiveness in load restoration. To enhance the resilience of active distribution systems, Ref. [19] employs multi-microgrids and mobile energy storage units (MSUs). The study proposes a framework for quantifying resilience and reveals the indispensability of MSUs for restoring critical loads under multiple-fault scenarios. Nevertheless, it is worth noting that the capacity of MSUs is predetermined artificially rather than optimized. Additionally, the obtained optimization solution is based on a single scenario rather than the predicted multiple scenarios.

In addition to enhancing system resilience, MES devices can also improve economic efficiency by reducing operational costs. Ref. [20] proposes a novel framework for enhancing energy cooperation within multi-island microgrids using marine MES (MMES). The results

suggest that MMES can provide substantial economic benefits. Similarly, Ref. [21] optimizes the node locations for MES connections to the grid at different times, leveraging its ability to smooth load fluctuations and facilitate renewable energy integration, which ultimately reduces the operating costs of active distribution networks. In addition to optimizing the operation of MES, Ref. [22] focuses on the deployment of mobile renewable energy charging stations, offering a dynamic and adaptable solution for charging MES devices.

Regarding short-term optimal scheduling methods for MES, Ref. [23] presents a stochastic optimization framework for microgrids that are equipped with diverse types of renewable-based distributed generators and plug-in electric vehicles (PEVs). The proposed framework effectively solves this problem through the implementation of a modified fluid search optimization algorithm. Similarly, Ref. [24] proposes a hierarchical stochastic optimization algorithm for energy management in NMGs with multiple energy sources, including microturbines, combined heat and power systems, hydrogen energy storage, battery energy storage, and PEVs. Notably, PEVs play a critical role in serving as energy sources to support on-fault islanded mobile energy microgrids (MEMGs), where they are scheduled by a central EMS. The results demonstrate a considerable enhancement in the resilience of the on-fault MEMGs. Furthermore, in Ref. [25], both the normal and emergency operation of electrochemical energy storage units are considered to reduce the operating costs and the number of shed loads. The simulation results presented in Ref. [18] exhibit how different scheduling strategies, based on various mobile generation units, improve both the resiliency criterion and the total cost.

1.2. Gaps and Contributions

Table 1 provides an overview of the relevant studies, highlighting key aspects that were overlooked in previous research. The following research gaps have been identified based on this review:

- Limited Objective Scope: Most studies derive their optimization results based on a single objective or a limited set of objectives, without considering a broader set of factors impacting system resilience.
- Insufficient Integration of MES and Dynamic Reconfiguration: A significant gap exists in the integration of MES deployment and dynamic boundary reconfiguration in response to natural-disaster-induced events. While some studies address the static placement of MES, they overlook the critical need for dynamic network reconfiguration in post-disaster scenarios.
- Overlooked MES Capacity–Economic Cost Relationship: The relationship between MES capacity and its economic cost is not adequately addressed in the literature. Specifically, there is a lack of simultaneous optimization of both MES capacity and deployment strategies.

To address these gaps, we have developed a novel two-stage stochastic programming framework for resilient NMGs with dynamic boundaries. This framework simultaneously considers the sizing, pre-positioning, and re-allocation of MES, allowing for dynamic reconfiguration of NMG boundaries using remote smart switches. This enables MES to be adaptively relocated, facilitating a flexible network topology that can accommodate evolving system conditions. Additionally, we have implemented a customized progressive hedging algorithm (PHA) to efficiently solve the two-stage stochastic programming problem. The main contributions of this paper, which directly address the identified research gaps, are summarized as follows:

- In this new problem, a scenario-based two-stage mixed-integer stochastic programming model is formulated. Specifically, the objectives are carefully chosen considering various dimensions, including reconfiguration time, effectiveness, operational constraints, and economic costs.

- A two-stage framework is proposed for the collaborative utilization of dynamic boundaries and mobile energy storage within NMGs. This framework enables real-time reconfiguration of the network topology and the adaptive re-allocation of MES.
- The proposed model simultaneously optimizes the sizing, pre-positioning, and re-allocation of MES, considering their economic costs. To the best of our knowledge, this is the first work to integrate these three aspects in the reconfiguration of NMGs.

The remainder of this paper is structured as follows. Section 2 describes the problem focused on in this paper. Sections 3 and 4 present the formulation of the first-stage and second-stage problems. Section 5 provides the customized progressive hedging algorithm. The results of simulation experiments are discussed in Section 6. Section 7 concludes this paper.

Table 1. A comparison of the relevant studies in the literature.

Ref.	Objectives				Considering Reconfiguration	Considering MES Usage	Considering MES Sizing	Test System
	Increase Supply Reliability	Minimize Economic Cost	Minimize Outage Duration	Minimize Power Exchange				
[9]	✓	×	×	×	✓	×	×	123-node
[10]	✓	×	×	×	✓	×	×	16-node
[11]	✓	✓	×	×	×	×	×	–
[12]	✓	×	✓	×	✓	×	×	123-node
[13]	✓	✓	×	✓	×	×	×	31-node
[14]	✓	✓	×	×	×	×	×	–
[15]	✓	×	×	×	×	×	×	144-node
[16]	✓	✓	×	×	×	×	×	33-node
[17]	✓	✓	×	×	✓	✓	×	118-node
[18]	✓	✓	×	×	×	✓	×	–
[19]	✓	✓	×	×	✓	✓	×	33-node
[20]	×	✓	×	×	×	✓	×	–
[21]	×	✓	×	×	×	✓	×	33-node
[26]	✓	✓	✓	×	×	×	×	123-bus
[27]	✓	×	×	×	×	✓	×	–
[28]	×	✓	×	✓	×	✓	×	–
[29]	×	✓	×	✓	×	✓	×	–
[30]	×	×	✓	×	✓	✓	×	37-node
This Paper	✓	✓	✓	✓	✓	✓	✓	33/69-node

2. Problem Description

The problem is an optimization problem of MES sizing, pre-positioning, and re-allocation for resilient NMGs with dynamic boundaries. After a natural-disaster-induced attack occurs, the distribution lines connecting to the microgrid may be damaged, which leads to power outages in the microgrid subsystems of the networked system. To mitigate the power outages resulting from these attacks, the resilient operations of NMG systems are proposed. On the one hand, the boundary of the microgrid subsystem can be adjusted, so that a subsystem with abundant power supply can support the damaged subsystem after line damage occurs; on the other hand, the MES devices are pre-positioned on the nodes with key load for rapid restoration, and the MES can be re-allocated to effectively balance the power supply across all microgrid subsystem regions. By optimizing the power flow and adjusting the boundaries within the NMG system, the overall system resilience can be returned to the highest level. Notably, the size capacity of MES is also a focus of this paper, and it is optimized to maximize cost-effectiveness.

As depicted in Figure 1, the problem includes two stages. In the first stage, before the natural disaster occurs, three MES devices are pre-positioned at suitable nodes based on the optimal solutions. Three boundary lines connect different microgrid subsystems with the switch status set to 'open'. In the second stage, after the damage event occurs, the

damaged lines will be detected, which are labeled with red crosses in the figure. The status of each boundary line switch is then determined accordingly. Meanwhile, the three MES devices are re-allocated to the optimal locations while coordinating with the adjustment of boundary line switch status. In the figure, eight new microgrid subsystems are formed to enable each node to receive power after the boundary adjustment of microgrid subsystems in the networked system.

This problem is based on five reasonable assumptions: (1) damage scenarios can be derived from expert knowledge or natural disaster damage models; (2) the system can rapidly detect damaged components and promptly update its status; (3) the amount of MES that can be pre-positioned at each node is limited; (4) all nodes are assumed to be reachable to one another; (5) hardened boundary lines are assumed to remain undamaged.

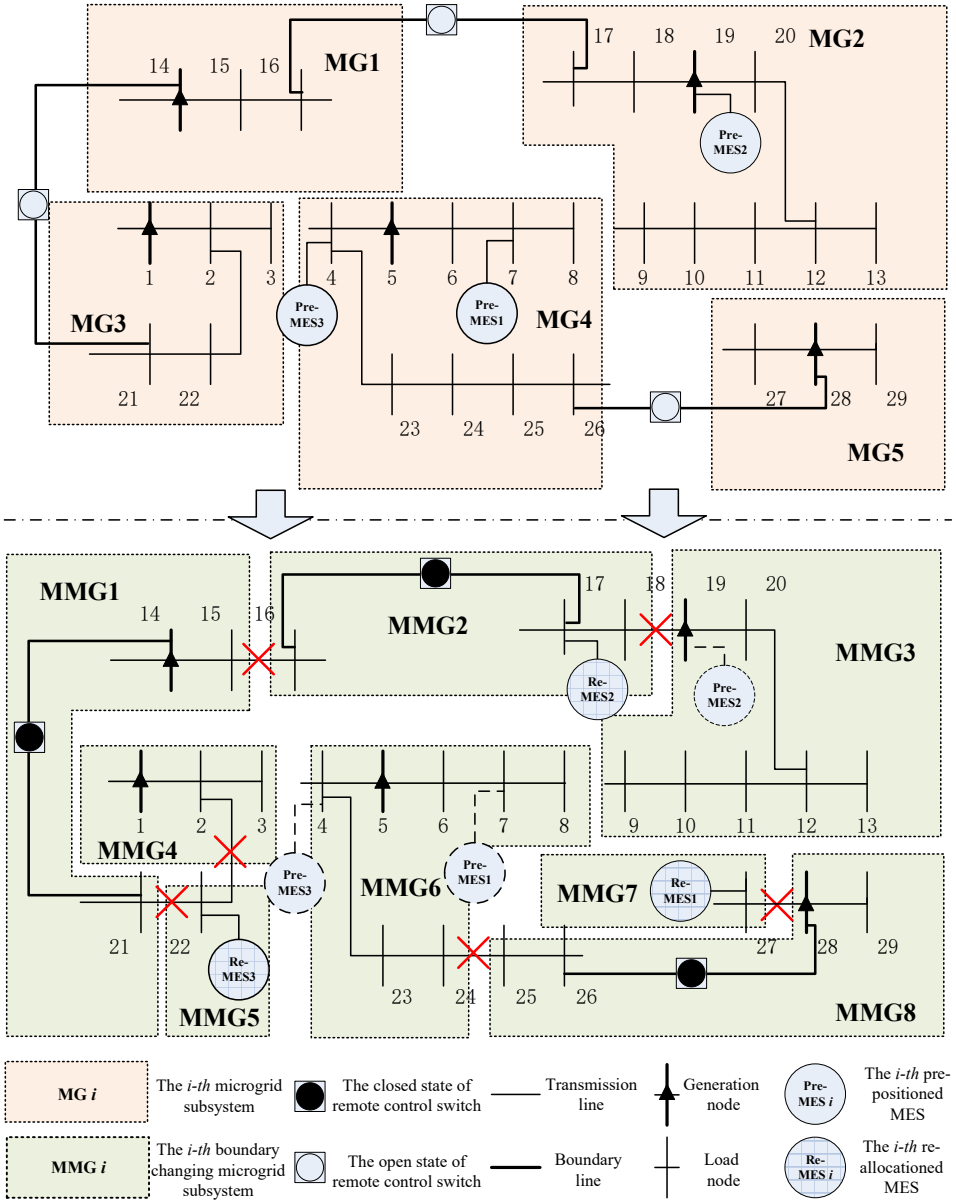


Figure 1. A schematic diagram of the proposed two-stage networked microgrid reconfiguration optimization method.

3. First-Stage Problem Formulation

In this section, the mathematical model of the problem is proposed.

3.1. Objective Function

In order to obtain a trade-off among the reconfiguration time, effectiveness, operational constraints, and economic costs, the objective function at the first (or pre-positioning) stage should take into account the outage time of loads, the number of loads to be shed, the number of switching operations, and the total purchasing capacity of MES, as illustrated in Equation (1). Since the four terms of the optimization objective have diverse dimensions, they are normalized and correspondingly labeled in the above equation. In essence, the outage time of loads is largely driven by the time required to re-allocate the MES (i.e., moving the pre-positioned MES to other nodes), denoted as $\sum_{p\in I_1}\sum_{k\in I_2}\sum_{m\in M}\beta_{mpkn}T_{skn}$, and the time required for operating the switches is a negligible factor. The aim at this stage is to pick up weighted loads as much as possible by using a strategy that minimizes the weighted loads to be shed, denoted as $\sum_{i\in I} Z_i sl_{in}$. Furthermore, the impact of the switching operations of boundary lines, measured based on the number of operations, $\sum_{(i,j)\in BL} bl_{ijn}$, is also considered. As the cost of MES devices is closely related to their battery capacity, it is economically preferred to minimize the total capacity of the purchased MES devices, represented as $\sum_{m\in M} G_m$. Though the problem is to efficiently restore as many loads as possible with the shortest time and lowest cost, the impact of switching operations and the weighting of each scenario W_n are also taken into consideration. The weights of four terms in the optimization objective, denoted as η_1 to η_4, are determined by the decision makers.

$$\min \sum_{n\in N} W_n \left\{ \eta_1 \frac{\sum_{p\in I_1}\sum_{k\in I_2}\sum_{m\in M}\beta_{mpkn}T_{skn}}{BM\cdot T_{\max}} + \eta_2 \frac{\sum_{i\in I} Z_i sl_{in}}{\sum_{i\in I} Z_i P_i} + \eta_3 \frac{\sum_{(i,j)\in BL} bl_{ijn}}{N_{bl}} + \eta_4 \frac{\sum_{m\in M} G_m}{BM\cdot G_M} \right\} \quad (1)$$

3.2. Constraints

The constraints of the model are as follows:

(1) MES pre-positioning constraints

Due to the limited capacity of each node, Constraint (2) indicates that the number of pre-positioned MES devices for each node cannot exceed its maximum capacity. Constraint (3) ensures that each MES device is pre-positioned at only one node.

$$\sum_{m\in M} \alpha_{mp} \le Np, \forall p \in I_1 \quad (2)$$

$$\sum_{p\in I_1} \alpha_{mp} = 1, \forall m \in M \quad (3)$$

(2) MES re-allocation constraints

Constraint (4) indicates that only if there is an MES device in the node at the first stage can the MES be dynamically re-allocated to the corresponding node in the second stage. Constraint (5) ensures that each MES device can only be re-sent from a pre-positioning node p to a re-allocation node k.

$$\sum_{k\in I_2} \beta_{mpkn} \le \alpha_{mp}, \forall p \in I_1, \forall m \in M, \forall n \in N \quad (4)$$

$$\sum_{p\in I_1}\sum_{m\in M} \beta_{mpkn} \le 1, \forall k \in I_2, \forall n \in N \quad (5)$$

(3) Topology reconfiguration constraints

The variables pm_{kn} and pf_{kn} represent whether there is an MES device re-allocated to node k and whether node k is a generation node under scenario n. The variable θ_{ij} indicates whether node j is the parent node of node i. Constraints (6) and (7) define a node as a power source node if it either receives power from an MES device or serves as a generation node. $|DL_n|$ denotes the number of damaged lines. Constraint (8) ensures that the number of damaged lines is equal to the predetermined budget. Constraints (9)–(11) guarantee that the reconfigured power system maintains a radial topology [31]. Specifically, Constraint (9) derives that θ_{ij} or θ_{ji} equals one (indicating a parent–child relationship between nodes i and j) if the status of the boundary line switch is closed or the distribution line is not damaged. It is noted that we assume that the distribution line is closed in all other states except for being damaged, and the boundary lines are hardened and will not be damaged in the second stage. Constraints (10) and (11) indicate each node has one or less parent node other than the power source nodes. The power source nodes include the generation nodes and the nodes connected to MES.

$$pm_{in} = \begin{cases} \sum_{s\in S}\sum_{m\in M} \beta_{msin} & ,i \in I_2, \forall n \in N \\ 0 & ,i \notin I_2, \forall n \in N \end{cases} \tag{6}$$

$$pf_{in} = \begin{cases} 1, i \in F, \forall n \in N \\ 0, i \notin F, \forall n \in N \end{cases} \tag{7}$$

$$|DL_n| = BD, \forall n \in N \tag{8}$$

$$\theta_{ijn} + \theta_{jin} = tl_{ijn} + bl_{ijn}, \forall i, j \in I, \forall n \in N \tag{9}$$

$$\sum_{j\in\psi(i)} \theta_{ijn} \le 1 - pm_{in}, \forall i \notin F, \forall n \in N \tag{10}$$

$$\theta_{ijn} = 0, \forall i \in F, j \in \psi(i), \forall n \in N \tag{11}$$

(4) Power balance constraints

Constraint (12) ensures that the inflow and outflow on node i are equal to achieve power balance. Constraint (13) determines the power flow according to the node phase angle and line state. If the line is not damaged, the value of $(bl_{ijn} + tl_{ijn})(1 - al_{ijn})$ is 1; otherwise, it is 0. Note that this term is nonlinear, and a binary variable λ_{ijn} is introduced to replace the term. Therefore, Equation (13) can be equivalently transformed into Equations (19) and (20) by the big-M method. "M" represents a considerably large numerical value. Constraint (14) guarantees that the value of shed loads on the node is between 0 and the power demand of the node. Constraints (15) and (16) indicate that the actual power generation of MES and the generation node cannot exceed their maximum power generation, respectively. Specifically, the value of gm_{imn} is determined by two factors; one is whether the node i is powered by MES m under scenario n (γ_{imn}), and the other is the purchasing capacity of MES m (G_m). Constraint (16) shows the two possibilities of the value of γ_{imn}.

$$gm_{imn} + gf_{in} - \sum_{l_{ij}|o(l_{ij})=i} p_{l_{ijn}} + \sum_{l_{ij}|d(l_{ij})=i} p_{l_{ijn}} + sl_{in} - P_i = 0, \forall i \in I, \forall m \in M, \forall n \in N \tag{12}$$

$$p_{l_{ijn}} r_{l_{ij}} = (bl_{ijn} + tl_{ijn})(1 - al_{ijn})(\delta_{o(l_{ij})} - \delta_{d(l_{ij})}), \forall i, j \in I, \forall n \in N \tag{13}$$

$$0 \le sl_{in} \le P_i, \forall i, \forall n \tag{14}$$

$$0 \le gm_{imn} \le \gamma_{imn} G_m, \forall i \in I, \forall m \in M, \forall n \in N \tag{15}$$

$$\gamma_{imn} = \begin{cases} \sum_{p\in I_1} \beta_{mpin} & ,\forall i \in I_2, \forall m \in M, \forall n \in N \\ 0 & ,\forall i \notin I_2, \forall m \in M, \forall n \in N \end{cases} \tag{16}$$

$$0 \le gf_{in} \le pf_{in} G_F, \forall i \in I, \forall n \in N \tag{17}$$

$$G_m \le G_M, \forall m \in M \tag{18}$$

$$-M(1-\lambda_{ijn})) \le \phi_{ijn} - (\delta_{o(l_{ij})} - \delta_{d(l_{ij})}) \le M(1-\lambda_{ijn}), \forall i,j \in I, \forall n \in N \quad (19)$$

$$-M\lambda_{ijn} \le \phi_{ijn} \le M\lambda_{ijn}, \forall i,j \in I, \forall n \in N \quad (20)$$

(5) Line state constraints

DL_n represents the set of damaged lines under scenario n. Constraints (21) and (22) restrict them so that they are inoperable in the open state. Constraints (21) and (23) indicate that if a node pair (i,j) is not included in the set of distribution lines or boundary lines, the variables representing their line state are set to 0.

$$tl_{ijn} = 0, \forall (i,j) \in DL_n \text{ or } \forall (i,j) \notin TL, \forall n \in N \quad (21)$$

$$al_{ijn} = 1, \forall (i,j) \in DL, \forall n \in N \quad (22)$$

$$bl_{ijn} = 0, \forall (i,j) \notin BL, \forall n \in N \quad (23)$$

4. Second-Stage Problem Formulation

In the first stage, the pre-positioning decisions (α_{mp}) and actual purchasing capacity (G_m) of each MES device are determined. In the second stage, according to the damaged lines in the actual damage scenario after the attack of a natural disaster, the MES devices are dynamically re-allocated (β_{mpkn}), and the switch operation of boundary lines (bl_{ijn}) is conducted. Moreover, the power flow of each line ($p_{l_{ijn}}$) and the output of each MES device (gm_{imn}) are optimized. The optimization goal of this stage is to minimize the cost in Equation (1) under scenario $\bar{n}$. The objective function is described as follows:

$$\min \left\{ \eta_1 \frac{\sum_{p\in I_1}\sum_{k\in I_2}\sum_{m\in M}\beta_{mpkn}T_{skn}}{BM \cdot T_{\max}} + \eta_2 \frac{\sum_{i\in I} Z_i sl_{in}}{\sum_{i\in I} Z_i P_i} + \eta_3 \frac{\sum_{(i,j)\in BL} bl_{ijn}}{N_{bl}} + \eta_4 \frac{\sum_{m\in M} G_m}{BM \cdot G_M} \right\}_{n=\bar{n}} \quad (24)$$

The objective defined in the second stage is subject to a subset of the aforementioned constraints, with the variation occurring under scenario $\bar{n}$, which are listed as follows.

$$\text{s.t. } (4)\text{–}(23),\ n = \bar{n}$$

5. Solving Method

Since the decision-making process of the NMG optimization model built in this paper is divided into two stages, and the objective function includes the binary variables β_{mpkn} and bl_{ijn} and the continuous variable sl_{in}, this problem is essentially a multi-stage mixed-integer stochastic programming problem. The information about the damage scenario is uncertain, which makes it difficult to solve the problem in a short period of time. Refs. [32,33] use the common approach of scenario generation to represent information uncertainty, which involves generating a predetermined number of scenarios with corresponding probabilities and uncertainty parameters. The uncertain parameters in this paper include the location of damaged lines, the priority weight of nodes, etc.

The progressive hedging algorithm has been proven to be an effective method for solving multi-stage stochastic programming problems [25,34], especially for problems with discrete decision variables at each stage [35]. Therefore, this algorithm is implemented in the Gurobi solver to solve the proposed two-stage stochastic programming problem based on scenario generation. The stochastic programming model in this paper can be summarized in the following form:

$$\min_{x,y} TC = c^T x + \sum_{\omega\in\Omega} \Pr(\omega) d_\omega^T y_\omega \quad (25)$$

$$\text{s.t. } (x, y_\omega) \in \mathcal{Q}_\omega, \forall \omega \in \Omega \quad (26)$$

where the decision vector x denotes the first-stage variables which represent the "here and now" decisions, such as the pre-positioning decisions (α_{mp}) and capacity purchasing

schemes of MES devices (G_m), and y_ω denotes the second-stage variables which represent the "wait and see" recourse actions determined by a given x and a certain scenario ω, such as the re-allocation decisions (β_{mpkn}) and switch operation schemes of boundary lines (bl_{ijn}). Vectors c and d_ω denote the coefficients corresponding to the aforementioned variables, and Ω is the set of scenarios. Restriction (26) represents the feasible region of decision variables x and y_ω in scenario ω with some constraints, i.e., Constraints (2)–(23). With the non-anticipativity constraints (29) enforcing the first-stage decision in every scenario being the same, the primary problem can be equivalently transformed to (27) and (28) to utilize duality theory.

$$\min_{x_\omega, y_\omega} TC = \sum_{\omega \in \Omega} \Pr(\omega)(c^T x_\omega + d_\omega^T y_\omega) \tag{27}$$

$$\text{s.t. } (x_\omega, y_\omega) \in \mathcal{Q}_\omega, \forall \omega \in \Omega \tag{28}$$

$$x_1 = \cdots x_\omega, \forall \omega = 1, \ldots, |\Omega| \tag{29}$$

Based on duality theory, the best lower bound can be obtained by solving the following problem:

$$TC \geq \max_{\delta} \left\{ \min_{x, \hat{x}, y} \sum_{\omega \in \Omega} \Pr(\omega)(c^T x_\omega + d_\omega^T y_\omega + \delta^T (x_\omega - \hat{x}) + \rho/2 \parallel x - \hat{x} \parallel_2^2) \right\} \tag{30}$$

$$\text{s.t. } \sum_{\omega \in \Omega} \Pr(\omega)\delta_\omega = 0, (x_\omega, y_\omega) \in \mathcal{Q}_\omega, \forall \omega \in \Omega \tag{31}$$

where $\hat{x}$ is a new vector variable of first-stage decisions for finding a solution with the same constraints, and ρ is a penalty parameter. The steps of PHA are described in Algorithm 1.

Algorithm 1: Progressive Hedging Algorithm

1 Initialization: Let k=0, δ^0=0 ;
2 **for** *all* $\omega \in \Omega$ **do**
3 | Solve $(x_\omega^1, y_\omega^1) = \underset{x_\omega, y_\omega}{\operatorname{argmin}} (c^T x_\omega + d_\omega^T y_\omega) : (x_\omega, y_\omega) \in \mathcal{Q}_\omega)$
4 **end**
5 k:=k+1;
6 **for** *all* $\omega \in \Omega$ **do**
7 | $\hat{x}^k = \sum_{\omega \in \Omega} \Pr(\omega) x_\omega^k$
8 | $\delta_\omega^k = \delta_\omega^{k-1} + \rho\left(x_\omega^{k-1} - \hat{x}^{k-1}\right)$
9 | $x_\omega^{k+1} = \min_{x_\omega, y_\omega} \{c^T x_\omega + d_\omega^T y_\omega + \delta^T x_\omega + \rho/2 \parallel x_\omega - \hat{x} \parallel_2^2\}$
10 | **if** $k > k_{max}$ *or* $\sqrt{\sum_{\omega \in \Omega} \Pr(\omega)\left(x_\omega^{k+1} - \hat{x}\right)^2} < \epsilon$ **then**
11 | | Return $\hat{x}^k$,x_ω^{k+1},y_ω^{k+1}
12 | **end**
13 **end**

The PHA essentially utilizes a scenario-based decomposition method, and it starts by solving the values of the first- and second-stage variables under every scenario in the first iteration in Step 2. During each iteration after the first, the expected value of x_ω^k (i.e., $\hat{x}^k$) and the multiplier δ_ω^k are updated in Steps 7 and 8, and then, the value of x_ω^{k+1} can be calculated in Step 9. The algorithm will terminate if the maximum number of iterations or termination threshold ϵ is reached. The term $\sqrt{\sum_{\omega \in \Omega} \Pr(\omega)\left(x_\omega^{k+1} - \hat{x}\right)^2} < \epsilon$ means the convergence is guaranteed, i.e., all first-stage decisions are non-anticipative.

6. Case Studies

In this section, we conduct numerical experiments on the proposed model and algorithm.

6.1. Experimental Design

The modified IEEE-33 and IEEE-69 node distribution systems [36,37] are employed as the test systems in this study. The modified IEEE-33 node distribution system comprises 33 nodes, including 5 generation nodes and 28 load nodes, interconnected by 32 lines. These lines comprise 28 branch lines and 4 boundary lines, as illustrated in Figure 2. Similarly, the modified IEEE-69 node distribution system consists of 69 nodes, which include 6 generation nodes and 63 load nodes, interconnected by 68 lines. These lines compass 63 branch lines and 5 boundary lines, as depicted in Figure 3. In this study, it is assumed that only the boundary lines are equipped with remote control switches, which are initially set to a default state of disconnection. The distribution lines are set to a default state of closed. The reactance ($r_{l_{ij}}$) of lines and power demand (P_i) at the nodes are adopted from the original data of the systems [36,37]. Further details regarding other data settings are provided in the following subsections.

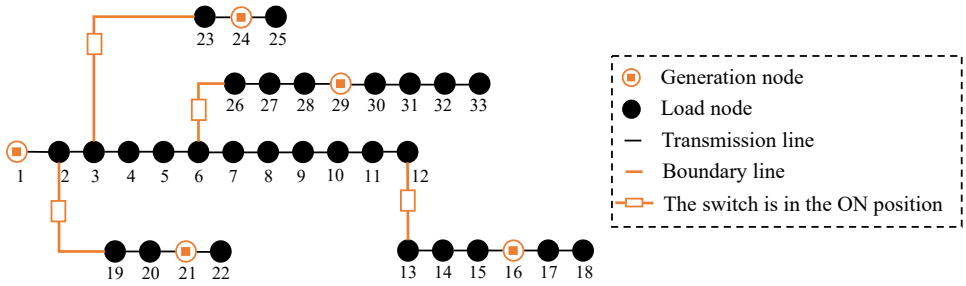


Figure 2. A modified IEEE 33-node test system.

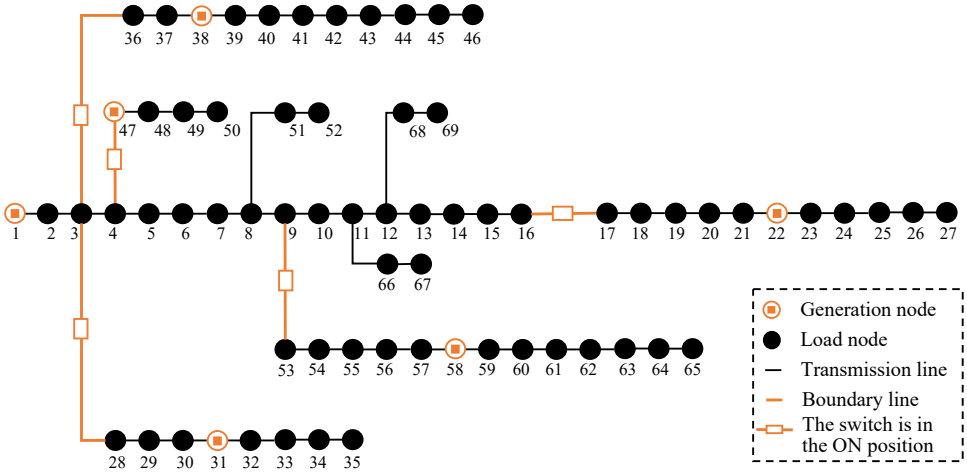


Figure 3. A modified IEEE 69-node test system.

6.2. Case I: Modified IEEE 33-Node Distribution System

The modified IEEE 33-node distribution system undergoes modifications through the reservation of certain lines and the alteration of node characteristics and distribution lines. Consequently, this system comprises five independent microgrid subsystems when the switches on boundary lines are in the open state. The capacities of the five generation nodes are listed in the first two columns of Table 2. Given the unavailability of actual damage data, this paper employs a normal distribution to generate ten hypothetical damage scenarios, as depicted in Table 3. The load priorities and transportation speeds of MES are randomly assigned from the sets $\{5, 3, 1\}$ and {60 km/h, 90 Kkm/h, 100 km/h}, respectively, with equal probabilities. The maximum purchasing capacity of the MES is set to 1000 kW.

Subsequently, the transportation time for each MES device along the designed routes is computed based on the fixed speed parameters and their Euclidean distances.

Table 2. The capacity of generation nodes of the modified IEEE 33/69-node distribution system.

IEEE 33-Node		IEEE 69-Node	
Generation node	Capacity (kW)	Generation node	Capacity (kW)
1	10,000	1	10,000
16	800	22	1000
21	600	31	1000
24	1300	38	1000
29	1300	47	3000
\	\	58	5000

Table 3. Samples of the damaged lines for the 10 generated scenarios using the normal distribution.

Scenario 1	Scenario 2	Scenario 3	Scenario 4	...	Scenario 10
Line (1, 2)	Line (1, 2)	Line (1, 2)	Line (6, 7)	...	Line (1, 2)
Line (6, 7)	Line (3, 4)	Line (3, 4)	Line (7, 8)	...	Line (14, 15)
Line (9, 10)	Line (7, 8)	Line (19, 20)	Line (11, 12)	...	Line (16, 17)
Line (21, 22)	Line (14, 15)	Line (23, 24)	Line (16, 17)	...	Line (23, 24)
Line (24, 25)	Line (16, 17)	Line (30, 31)	Line (21, 22)	...	Line (24, 25)
Line (32, 33)	Line (30, 31)	Line (32, 33)	Line (28, 29)	...	Line (27, 28)

Taking Scenario 1 of Table 3 as an example, we illustrate the application of the proposed two-stage optimization method. Prior to the occurrence of natural disasters, the optimal pre-positioning and capacity purchase schemes for MES devices are determined by solving the first-stage problem using the ten generated scenarios, as shown in the second columns of Tables 4 and 5. The first-stage solutions aim to optimize the effectiveness of the MES allocation scheme in the second stage. Notably, Table 5 reveals that the purchased capacities of the three MES devices are smaller than the maximum design capacity (1000 kW), demonstrating noticeable economic benefits. In Figure 4, the nodes connected to quadrangular-star nodes denote the presence of MES devices. From Figure 4a, it can be observed that the MES devices are pre-positioned on nodes 7, 18, and 31 in the first stage.

Table 4. The pre-positioning and re-allocation scheme of MES devices in Case I.

MES	Pre-Positioning Nodes		Re-Allocation Nodes
I	node 7	→	node 7
II	node 18	→	node 22
III	node 31	→	node 33

Table 5. Capacity Utilization of MES devices in Case I.

MES	Energy Storage Size (kW)		Power Output (kW)	Utilization Rate (%)
I	800	→	460	57.50%
II	300	→	90	30.00%
II	420	→	60	14.29%

Upon the occurrence of a natural disaster, the damaged lines in the actual scenario are detected and marked with a cross in Figure 4b. The optimal re-allocation scheme for MES is derived by solving the second-stage problem using the selected reality scenario. Subsequently, the MES devices are dispatched from the pre-positioning nodes to the re-allocation nodes, with the corresponding decisions listed in the forth column of Table 4. Once the MES devices arrive at the re-allocation nodes, they are integrated into the system

as source nodes. Figure 4b illustrates that MES II and III are dispatched to re-allocation nodes 22 and 33, respectively, while MES I remains stationed at pre-positioning node 7, adhering to the proximity principle. Additionally, as shown in Table 6, the switches on the boundary lines (3, 23) and (12, 13) are turned off. Consequently, most of the load nodes are restored as several microgrid subsystem are formed, with the exception of node 25. As the boundaries expand, the node sets $\{3, 4, 5, 6\}$ and $\{10, 11, 12\}$ transition from being powered by generation node 1 to being powered by generation nodes 24 and 16, respectively.

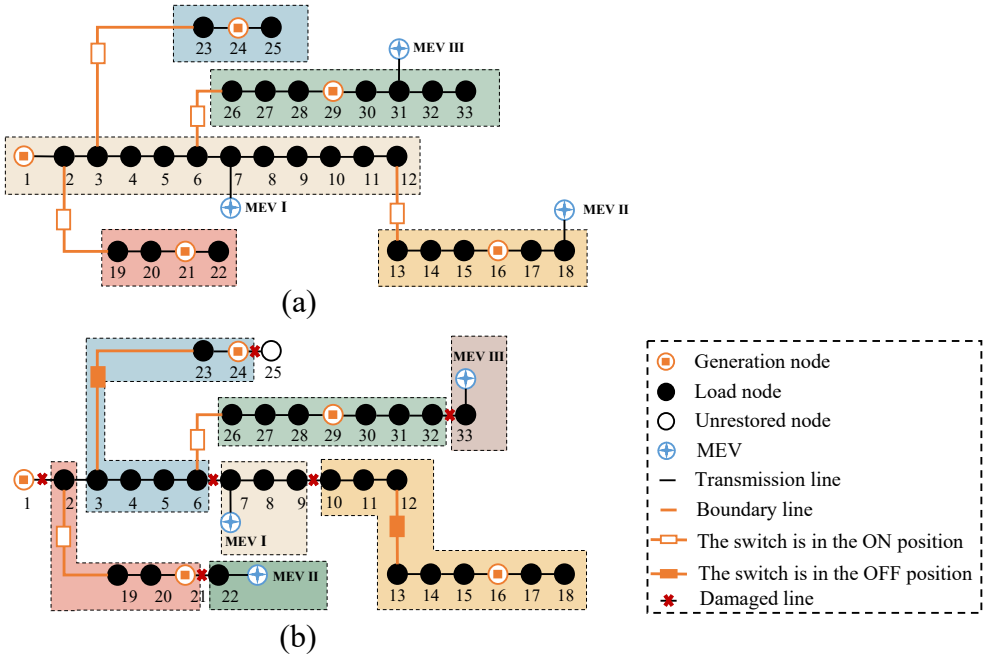


Figure 4. The optimization solution for the modified IEEE 33-node distribution system. (**a**) The first stage. (**b**) The second stage.

Table 6. The switch operation scheme of boundary lines in Case I.

Boundary Line	First Stage		Second Stage
Line (2, 19)	open	→	open
Line (3, 23)	open	→	closed
Line (6, 26)	open	→	open
Line (12, 13)	open	→	closed

6.3. Case II: Modified IEEE 69-Node Distribution System

As shown in Figure 3, the modified IEEE 69-node test case is used to examine the scalability of the proposed method for larger networks. The case of the IEEE 69-node distribution system is modified by replacing five load nodes with generation nodes, and substituting five distribution lines with boundary lines. Thus, when the boundary lines are disconnected, the system comprises six independent microgrid subsystems. The capacities of the five added generation nodes are listed in the last two columns of Table 2. While the capacity of node 1 is obtained from the original system data, the capacities of the other five nodes are related to the power demands of the load nodes within their corresponding microgrid subsystems. The parameters associated with MES devices are similar to those in Case I.

It is assumed that there are four MES devices and ten arbitrarily selected damaged lines, labeled in Figure 5. The pre-positioning and re-allocation scheme of MES devices and the utilization of their capacities are detailed in Tables 7 and 8, respectively. Figure 5 illustrates that in the first stage, the MES devices are pre-positioned at nodes 17,

65, 7, and 45. In the second stage, MES I, III, and IV are re-allocated to nodes 21, 50, and 56, respectively, while MES II remains stationed at node 65, resulting in the formation of nine microgrid subsystems. Additionally, as shown in Table 9, the switches on boundary lines (9, 53) and (16, 17) are turned off. Consequently, the nodes in sets {9–17, 53–56, 66–69} are reconnected to new power sources, as the boundaries are changed.

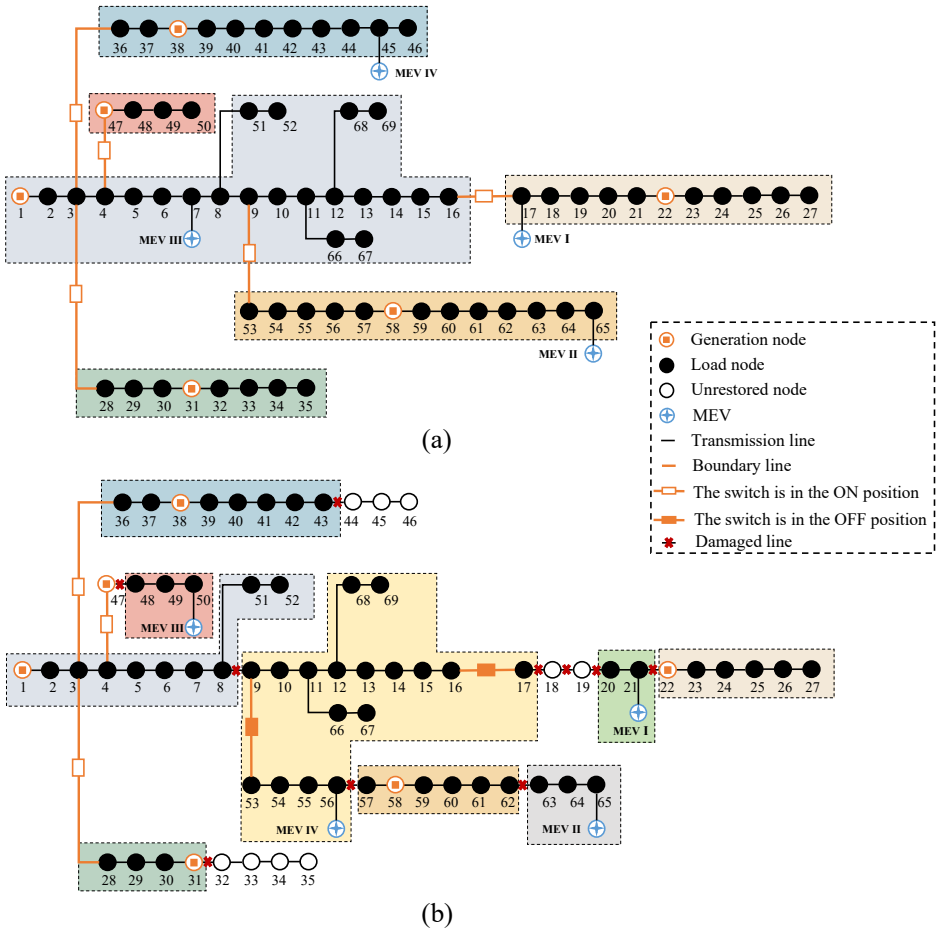


Figure 5. The optimization solution for the modified IEEE 69-node distribution system. (**a**) The first stage. (**b**) The second stage.

Table 7. The pre-positioning and re-allocation scheme of MES devices in Case II.

MES	Pre-Positioning Nodes		Re-Allocation Nodes
I	node 17	→	node 21
II	node 65	→	node 65
III	node 7	→	node 50
IV	node 45	→	node 56

Table 8. Capacity Utilization of MES devices in Case II.

MES	Energy Storage Size (kW)		Power Output (kW)	Utilization Rate (%)
I	605	→	115	19.01%
II	1000	→	286	28.60%
III	1000	→	848.4	84.84%
III	650	→	616.2	94.80%

Table 9. The switch operation scheme of boundary lines in Case II.

Boundary Line	First Stage		Second Stage
Line (3, 28)	open	→	open
Line (3, 36)	open	→	open
Line (4, 47)	open	→	open
Line (9, 53)	open	→	closed
Line (16, 17)	open	→	closed

6.4. Impact of Microgrid Boundary Lines

As described in the above two cases, the boundary lines play an essential role in microgrid reconfiguration, where the switches of boundary lines can form microgrid subsystems dynamically. To better illustrate the superiority of dynamic boundary lines, comparisons are conducted between the proposed model and a model without boundary lines, where the compared model is represented by several stand-alone microgrids. Based on the proposed two-stage optimization framework, the objectives of this compared model are presented in Equations (32) and (33), followed by the constraints that need to be satisfied. We use the same damage scenarios in Case II to examine the model without boundary lines; the optimization results are shown in Figure 6. It can be seen from Figure 6 that more loads need to be shed compared to the results in Case I. Apart from node 25 remaining unpowered, the nodes in set $\{10, 11, 12, 22\}$ are also without electricity supply.

$$\min \sum_{n\in N} W_n \left\{ \eta_1 \frac{\sum_{p\in I_1}\sum_{k\in I_2}\sum_{m\in M} \beta_{mpkn} T_{skn}}{BM \cdot T_{\max}} + \eta_2 \frac{\sum_{i\in I} Z_i sl_{in}}{\sum_{i\in I} Z_i P_i} + \eta_3 \frac{\sum_{m\in M} G_m}{BM \cdot G_M} \right\} \tag{32}$$

$$\min \left\{ \eta_1 \frac{\sum_{p\in I_1}\sum_{k\in I_2}\sum_{m\in M} \beta_{mpkn} T_{skn}}{BM \cdot T_{\max}} + \eta_2 \frac{\sum_{i\in I} Z_i sl_{in}}{\sum_{i\in I} Z_i P_i} + \eta_3 \frac{\sum_{m\in M} G_m}{BM \cdot G_M} \right\} \tag{33}$$

$$\theta_{ijn} + \theta_{jin} = tl_{ijn}, \forall i, j \in I, \forall n \in N \tag{34}$$

$$p_{l_{ijn}} r_{l_{ij}} = tl_{ijn}(1 - al_{ijn})(\delta_{o(l_{ij})} - \delta_{d(l_{ij})}), \forall i, j \in I, \forall n \in N \tag{35}$$

$$\text{s.t. } (2)\text{–}(8), (10)\text{–}(12), (14)\text{–}(18), (21)\text{–}(22)$$

Furthermore, as summarized in Tables 10 and 11, the optimization process based on both of the models is simulated for 20 rounds under different damage scenario settings. To assess the effects, load shedding is employed and measured by using Equation (36). $|N|$ denotes the number of scenarios. The results of the two tables clearly indicate that the model without boundary lines produces higher load shedding compared to the proposed model with boundary lines. Moreover, when the experimental parameters shift towards conditions unfavorable for optimization, such as an increase in damaged line number and a decrease in MES budget, it makes sense that the proposed model with boundary lines exhibits a smaller increase in load shedding compared to the model without boundary lines. This observation further confirms the superior robustness of the model with boundary lines. Overall, these results demonstrate that by operating the switches on boundary lines, each microgrid subsystem is capable of expanding its boundaries to interconnect with other microgrid subsystems and form NMGs, thus achieving energy mutual assistance and reducing the shed loads.

$$\text{Load Shedding} = \frac{\sum_{n\in N} \left(\sum_{i\in I} Z_i sl_{in} / \sum_{i\in I} Z_i P_{in} \right)}{|N|} \times 100\%, \forall i \in I \tag{36}$$

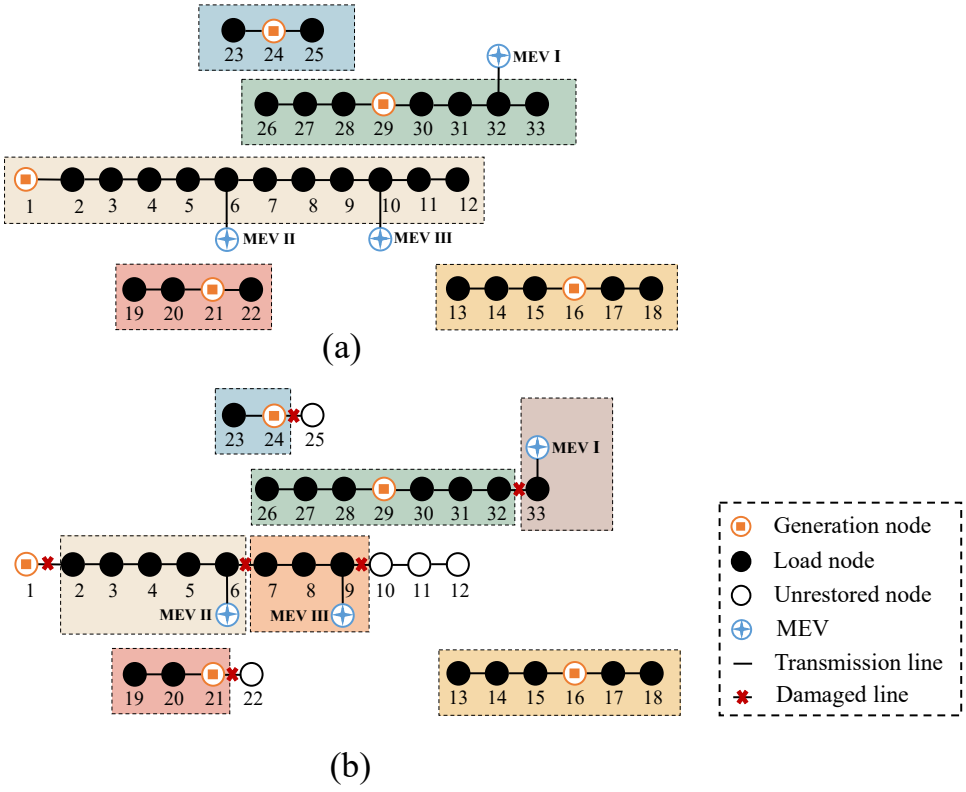


Figure 6. The optimization solution for the modified IEEE 33-node distribution system without boundary lines. (**a**) The first stage. (**b**) The second stage.

Table 10. Statistical simulations for load shedding under varying budgets of MES devices.

Budgets of Damaged Lines	Budgets of MES Devices	Load Shedding (%)	
		With Boundary Lines	Without Boundary Line
8	1	26.92%	35.70%
8	2	17.65%	26.37%
8	3	10.47%	18.32%
8	4	6.71%	13.72%

Table 11. Statistical simulations for load shedding under varying budgets of damaged lines.

Budgets of Damaged Lines	Budgets of MES Devices	Load Shedding (%)	
		With Boundary Lines	Without Boundary Line
6	3	5.32%	11.85%
7	3	8.10%	15.04%
8	3	10.47%	18.32%
9	3	13.49%	22.08%

6.5. Impact of MES Sizing

This subsection investigates the capacity utilization of MES devices to measure the effectiveness of MES sizing. As shown in Equation (37), CUR is proposed as an evaluation index, which is equal to the average of the actual power output of each MES divided by the corresponding purchased energy storage size. Further, we provide another index, $CUR^{'}$, where G_m in CUR is replaced by the maximum design capacity G_M, as shown in Equation (38).

$$\text{CUR} = \left(\frac{\sum_{m \in M} gm_{imn} / G_m}{BM} \right) \times 100\%, \forall i \in I, \forall n \in N \tag{37}$$

$$\text{CUR}' = \left(\frac{\sum_{m \in M} gm_{imn} / G_M}{BM} \right) \times 100\%, \forall i \in I, \forall n \in N \tag{38}$$

Based on the setting parameters of MES devices and damage scenarios discussed in Section 6.3, we perform 20 rounds of simulation of the networked microgird optimization and calculate the average value of the two indexes. The statistics for average CUR and CUR′ are listed in the third and forth columns of Tables 12 and 13. As the results show, the value of average CUR consistently surpasses that of average CUR′. In particular, as the budget of MES devices increases, the value of average CUR remains relatively stable, exhibiting a smaller decline for that of average CUR′. In general, the proposed capacity sized model demonstrates higher capacity utilization compared to a non-sized model. This advantage becomes particularly pronounced as the budget of MES devices increases, thereby implying superior economic benefits.

Table 12. Simulation statistics for average CUR under varying budgets of MES devices.

Budgets of Damaged Lines	Budgets of MES Devices	Average CUR	Average CUR′
8	1	49.63%	34.44%
8	2	49.10%	32.97%
8	3	49.03%	29.43%
8	4	46.24%	24.39%

Table 13. Simulation statistics for average CUR under varying budgets of damaged lines.

Budgets of Damaged Lines	Budgets of MES Devices	Average CUR	Average CUR′
6	3	46.89%	27.42%
7	3	47.09%	30.40%
8	3	49.03%	29.43%
9	3	50.57%	30.98%

6.6. Computational Efficiency

In this paper, the proposed two-stage stochastic mixed-integer linear programming problem is solved on a personal computer equipped with an Intel Core i7 processor (2.60 GHz) with 64 GB RAM, using Gurobi 11.0.1 with its default settings. The termination threshold for Algorithm 1 is set at 0.1%.

Table 14 compares the computation time between the PHA and directly using Gurobi 11.0.1 (with the MIPGap set to 0.1% for a fair comparison) across varying numbers of scenarios. In the modified IEEE 33-node system, 8 damaged lines are considered with 2 MES devices deployed, while in the modified IEEE 69-node system, 12 damaged lines are considered with 3 MES devices deployed. The results show that as the number of scenarios and problem size increase, the solution time grows for both methods. Notably, in the 69-node system, the computation time for Gurobi increases significantly when the number of scenarios reaches 20. In contrast, the PHA achieves a substantial reduction in solution time compared to using Gurobi directly. By decomposing the main problem into scenario-based subproblems, the PHA effectively reduces the computational load as the number of scenarios increases. However, although a larger number of scenarios improves solution quality, it also increases computation time, making the selection of an appropriate number of scenarios a crucial consideration.

Table 14. Comparison of computation time (minutes) for problem solving.

Power System	Solution Method	Scenario Number		
		10	20	30
33-node	Gurobi 11.0.1	0.22	1.34	4.57
	PHA	0.19	0.96	3.06
69-node	Gurobi 11.0.1	15.63	140.13	379.22
	PHA	7.88	79.91	252.80

7. Conclusions

This paper proposes a two-stage stochastic mixed-integer model for the restoration of NMGs,which simultaneously optimizes the sizing, pre-positioning, and reallocation of MES devices, as well as the dynamic reconfiguration of NMG boundaries. Our numerical studies on the modified IEEE 33-node and 69-node distribution systems demonstrate the effectiveness, robustness and economic benefits of the proposed model and algorithm. The main research results are summarized as follows:

(1) Simultaneous Pre-Disaster Optimization: The proposed approach enables the joint optimization of MES capacity and pre-positioning before a disaster occurs. This not only enhances system resilience, but also significantly reduces economic costs. By providing a comprehensive strategy for pre-disaster planning, it offers decision makers a valuable tool for developing proactive prevention measures.

(2) Post-Disaster Reallocation and Dynamic Boundary Reconfiguration: After a disaster, the re-allocation of MES devices and the operation of boundary switches can dynamically adjust the operational boundaries of microgrids. This flexibility allows previously isolated microgrids to reconnect to power sources, forming new NMGs. As a result, the risk of prolonged isolation is mitigated, and overall system resilience is greatly enhanced.

(3) Effectiveness of the Customized PHA: The customized PHA employed in this study proves highly effective in addressing multi-stage stochastic programming problems. It demonstrates strong performance in optimizing complex, uncertain scenarios, making it a suitable method for solving large-scale problems in power systems.

Several promising areas for future research are worth investigating to further enhance the proposed framework. First, incorporating more detailed and realistic disaster damage scenarios, tailored to different types of natural disasters, would be beneficial. By generating representative disaster patterns, more accurate modeling of post-disaster recovery and resource allocation strategies can be achieved. Additionally, deeper integration with transportation networks, coupled with the coordination of repair crews, should be explored. This would involve optimizing the scheduling of MES devices in conjunction with the sequence of repairing damaged components, ensuring a coordinated approach that improves the overall efficiency of the recovery process. Furthermore, the potential to leverage private electric vehicles (EVs) as supplementary mobile energy storage units warrants investigation. By integrating privately owned EVs into the framework, enhanced system flexibility can be achieved, particularly in scenarios where additional energy resources are limited during disaster recovery operations.

Author Contributions: Conceptualization, B.J. and H.L.; methodology, B.J. and H.L.; software, B.J. and C.Z.; validation, B.J. and Y.L.; formal analysis, B.J.; data curation, B.J.; writing—original draft preparation, B.J.; writing—review and editing, B.J., H.L., and Y.L.; visualization, B.J. and Y.L.; supervision, H.L. and C.Z.; project administration, T.Z. All authors have read and agreed to the published version of the manuscript.

Funding: This work was partly supported by the Hunan Provincial Natural Science Foundation of China under grant no. 2022JJ10069, and by the Hunan Provincial Science and Technology Innovation Program of China under grant no. 2023RC1002. This support is greatly appreciated.

Institutional Review Board Statement: Not applicable.

Informed Consent Statement: Not applicable.

Data Availability Statement: The original contributions presented in the study are included in the article, further inquiries can be directed to the corresponding authors.

Conflicts of Interest: The authors declare no conflicts of interest. The funders had no role in the design of the study; in the collection, analyses, or interpretation of data; in the writing of the manuscript; or in the decision to publish the results.

Abbreviations

Indices and Sets

I	Set of microgird nodes, $i, j \in I$.
I_1	Pre-positioning nodes for MES device connection in the first stage, $p \in I_1$.
I_2	Re-allocation nodes for MES device connection in the second stage, $k \in I_2$.
F	Set of generation nodes.
M	Set of MES devices, $m \in M$.
N	Set of scenarios, $n \in N$.
TL	Set of distribution lines, $l_{ij} \in TL$.
BL	Set of boundary lines, $l_{ij} \in BL$.
DL_n	Set of damaged lines under scenario n.

Parameters

N_g	Number of microgird nodes.
N_p	Maximum number of MES devices available at the pre-positioning node p.
N_{bl}	Number of boundary lines in the NMGs.
BM	Budget of MES devices .
BD	Budget of damaged distribution lines.
G_F	Capacity of generation nodes.
G_M	Maximum design capacity of MES devices.
T_{pkn}	Travel time of an MES device from pre-positioning node p to re-allocation node k under scenario n.
$r_{l_{ij}}$	Reactance of line l_{ij} .
$o(l_{ij})$	Origin node of line l_{ij}.
$d(l_{ij})$	Destination node of line l_{ij}.
W_n	Weight of scenario n.
Z_i	Priority weight of node i
P_i	Power demand at node i.
γ_i	Weight of the i-th objective.

Variables

G_m	Actual purchasing capacity of MES m.
gm_{imn}	Generation level of node i supported by MES m under scenario n.
gf_{in}	Generation level of generation node i under scenario n.
sl_{in}	Shed loads on node i under scenario n.
l_{ij}	Binary: 1 if there is a line connecting node i and node j, and 0 otherwise.
al_{ijn}	Binary: 1 if line (i, j) is attacked under scenario n, and0 otherwise.
bl_{ijn}	Binary: 1 if the switch on boundary line (i, j) is closed under scenario n, and 0 otherwise.
tl_{ijn}	Binary: 1 if the switch on distribution line (i, j) is closed under scenario n, and 0 otherwise.
α_{mp}	Binary: 1 if MES m is pre-positioned to node p, and 0 otherwise.
β_{mpkn}	Binary: 1 if MES m is re-allocated (sent) from node p to node k in real time under scenario n, and 0 otherwise.
γ_{imn}	Binary: 1 if MES m is re-allocated (sent) to node i in real time under scenario n, and 0 otherwise.
pm_{kn}	Binary: 1 if an MES device is connected to node k under scenario n, and 0 otherwise.
pf_{kn}	Binary: 1 if node k is a generation node under scenario n, and 0 otherwise.
$p_{l_{ijn}}$	Power flow of line l_{ij} under scenario n.
λ_{ijn}	Auxiliary binary variable to replace the nonlinear term $(bl_{ijn} + tl_{ijn})(1 - al_{ijn})$.
ϕ_{ijn}	Auxiliary continuous variable to replace the nonlinear term $\lambda_{ijn}(\delta_{o(l_{ij})} - \delta_{d(l_{ij})})$.

References

1. Bynum, M.; Staid, A.; Arguello, B.; Castillo, A.; Knueven, B.; Laird, C.D.; Watson, J.P. Proactive operations and investment planning via stochastic optimization to enhance power systems' extreme weather resilience. *J. Infrastruct. Syst.* **2021**, *27*, 04021004. [CrossRef]
2. Lee, C.C.; Maron, M.; Mostafavi, A. Community-scale big data reveals disparate impacts of the Texas winter storm of 2021 and its managed power outage. *Humanit. Soc. Sci. Commun.* **2022**, *9*, 1–12. [CrossRef] [PubMed]
3. Singh, A.R.; Raju, D.K.; Raghav, L.P.; Kumar, R.S. State-of-the-art review on energy management and control of networked microgrids. *Sustain. Energy Technol. Assess.* **2023**, *57*, 103248. [CrossRef]
4. Wang, Z.; Chen, B.; Wang, J.; Chen, C. Networked microgrids for self-healing power systems. *IEEE Trans. Smart Grid* **2015**, *7*, 310–319. [CrossRef]
5. Zhang, F.; Zhao, H.; Hong, M. Operation of networked microgrids in a distribution system. *CSEE J. Power Energy Syst.* **2015**, *1*, 12–21. [CrossRef]
6. Zamora, R.; Srivastava, A.K. Multi-layer architecture for voltage and frequency control in networked microgrids. *IEEE Trans. Smart Grid* **2016**, *9*, 2076–2085. [CrossRef]
7. Li, Z.; Shahidehpour, M.; Aminifar, F.; Alabdulwahab, A.; Al-Turki, Y. Networked microgrids for enhancing the power system resilience. *Proc. IEEE* **2017**, *105*, 1289–1310. [CrossRef]
8. Islam, M.; Yang, F.; Amin, M. Control and optimisation of networked microgrids: A review. *IET Renew. Power Gener.* **2021**, *15*, 1133–1148. [CrossRef]
9. Arif, A.; Wang, Z. Networked microgrids for service restoration in resilient distribution systems. *IET Gener. Transm. Distrib.* **2017**, *11*, 3612–3619. [CrossRef]
10. Qiu, D.; Wang, Y.; Wang, J.; Zhang, N.; Strbac, G.; Kang, C. Resilience-Oriented Coordination of Networked Microgrids: A Shapley Q-Value Learning Approach. *IEEE Trans. Power Syst.* **2023**, *39*, 3401–3416. [CrossRef]
11. Fesagandis, H.S.; Jalali, M.; Zare, K.; Abapour, M.; Karimipour, H. Resilient scheduling of networked microgrids against real-time failures. *IEEE Access* **2021**, *9*, 21443–21456. [CrossRef]
12. Arif, A.; Wang, Z. Service restoration in resilient power distribution systems with networked microgrid. In Proceedings of the 2016 IEEE Power and Energy Society General Meeting (PESGM), Boston, MA, USA, 17–21 July 2016; IEEE: New York, NY, USA, 2016; pp. 1–5.
13. Liang, Z.; Alsafasfeh, Q.; Su, W. Proactive resilient scheduling for networked microgrids with extreme events. *IEEE Access* **2019**, *7*, 112639–112652. [CrossRef]
14. Hussain, A.; Bui, V.H.; Kim, H.M. Resilience-oriented optimal operation of networked hybrid microgrids. *IEEE Trans. Smart Grid* **2017**, *10*, 204–215. [CrossRef]
15. Wang, Z.; Shen, C.; Xu, Y.; Liu, F.; Wu, X.; Liu, C.C. Risk-limiting load restoration for resilience enhancement with intermittent energy resources. *IEEE Trans. Smart Grid* **2018**, *10*, 2507–2522. [CrossRef]
16. Shaker, A.; Safari, A.; Shahidehpour, M. Reactive power management for networked microgrid resilience in extreme conditions. *IEEE Trans. Smart Grid* **2021**, *12*, 3940–3953. [CrossRef]
17. Mansouri, S.A.; Nematbakhsh, E.; Ahmarinejad, A.; Jordehi, A.R.; Javadi, M.S.; Marzband, M. A hierarchical scheduling framework for resilience enhancement of decentralized renewable-based microgrids considering proactive actions and mobile units. *Renew. Sustain. Energy Rev.* **2022**, *168*, 112854. [CrossRef]
18. Gargari, M.Z.; Hagh, M.T.; Zadeh, S.G. Preventive scheduling of a multi-energy microgrid with mobile energy storage to enhance the resiliency of the system. *Energy* **2023**, *263*, 125597. [CrossRef]
19. Mishra, D.K.; Ghadi, M.J.; Li, L.; Zhang, J.; Hossain, M. Active distribution system resilience quantification and enhancement through multi-microgrid and mobile energy storage. *Appl. Energy* **2022**, *311*, 118665. [CrossRef]
20. Wu, C.; Zhou, D.; Lin, X.; Sui, Q.; Wei, F.; Li, Z. A novel energy cooperation framework for multi-island microgrids based on marine mobile energy storage systems. *Energy* **2022**, *252*, 124060. [CrossRef]
21. Xia, S.; Wang, Z.; Gao, X.; Li, W. Optimal planning of mobile energy storage in active distribution network. *IET Smart Grid* **2024**, *7*, 1–12. [CrossRef]
22. Ala, A.; Deveci, M.; Bani, E.A.; Sadeghi, A.H. Dynamic capacitated facility location problem in mobile renewable energy charging stations under sustainability consideration. *Sustain. Comput. Inform. Syst.* **2024**, *41*, 100954. [CrossRef]
23. Hai, T.; Zhou, J.; Khaki, M. Optimal planning and design of integrated energy systems in a microgrid incorporating electric vehicles and fuel cell system. *J. Power Sources* **2023**, *561*, 232694. [CrossRef]
24. Ahmadi, S.E.; Marzband, M.; Ikpehai, A.; Abusorrah, A. Optimal stochastic scheduling of plug-in electric vehicles as mobile energy storage systems for resilience enhancement of multi-agent multi-energy networked microgrids. *J. Energy Storage* **2022**, *55*, 105566. [CrossRef]
25. Kim, J.; Dvorkin, Y. Enhancing distribution system resilience with mobile energy storage and microgrids. *IEEE Trans. Smart Grid* **2018**, *10*, 4996–5006. [CrossRef]
26. Kamal, F.; Chowdhury, B.H.; Lim, C. Networked microgrid scheduling for resilient operation. *IEEE Trans. Ind. Appl.* **2023**, *60*, 2290–2301. [CrossRef]
27. Wang, Y.; Rousis, A.O.; Qiu, D.; Strbac, G. A stochastic distributed control approach for load restoration of networked microgrids with mobile energy storage systems. *Int. J. Electr. Power Energy Syst.* **2023**, *148*, 108999. [CrossRef]

28. Wu, C.; Han, H.; Gao, S.; Liu, Y. Coordinated Scheduling for Multimicrogrid Systems Considering Mobile Energy Storage Characteristics of Electric Vehicles. *IEEE Trans. Transp. Electrif.* **2022**, *9*, 1775–1783. [CrossRef]
29. Qu, Z.; Chen, J.; Peng, K.; Zhao, Y.; Rong, Z.; Zhang, M. Enhancing stochastic multi-microgrid operational flexibility with mobile energy storage system and power transaction. *Sustain. Cities Soc.* **2021**, *71*, 102962. [CrossRef]
30. Lei, S.; Wang, J.; Chen, C.; Hou, Y. Mobile emergency generator pre-positioning and real-time allocation for resilient response to natural disasters. *IEEE Trans. Smart Grid* **2016**, *9*, 2030–2041. [CrossRef]
31. Jabr, R.A.; Singh, R.; Pal, B.C. Minimum loss network reconfiguration using mixed-integer convex programming. *IEEE Trans. Power Syst.* **2012**, *27*, 1106–1115. [CrossRef]
32. Ouyang, M.; Duenas-Osorio, L. Time-dependent resilience assessment and improvement of urban infrastructure systems. *Chaos Interdiscip. J. Nonlinear Sci.* **2012**, *22*, 033122. [CrossRef] [PubMed]
33. Winkler, J.; Duenas-Osorio, L.; Stein, R.; Subramanian, D. Performance assessment of topologically diverse power systems subjected to hurricane events. *Reliab. Eng. Syst. Saf.* **2010**, *95*, 323–336. [CrossRef]
34. Crainic, T.G.; Fu, X.; Gendreau, M.; Rei, W.; Wallace, S.W. Progressive hedging-based metaheuristics for stochastic network design. *Networks* **2011**, *58*, 114–124. [CrossRef]
35. Gade, D.; Hackebeil, G.; Ryan, S.M.; Watson, J.P.; Wets, R.J.B.; Woodruff, D.L. Obtaining lower bounds from the progressive hedging algorithm for stochastic mixed-integer programs. *Math. Program.* **2016**, *157*, 47–67. [CrossRef]
36. Maleh, M.S.; Nezhad, R.R.; Ghadimi, N. Placement of distributed generation units using multi objective function based on SA algorithm. *Sci. Res. Essays* **2013**, *8*, 1471–1477.
37. BaranME, W.F. Optimum sizing of capacitor placed on radial distribution systems. *IEEE Trans. PWRD* **1989**, *4*, 735–743.

Disclaimer/Publisher's Note: The statements, opinions and data contained in all publications are solely those of the individual author(s) and contributor(s) and not of MDPI and/or the editor(s). MDPI and/or the editor(s) disclaim responsibility for any injury to people or property resulting from any ideas, methods, instructions or products referred to in the content.